IEEE Access
Multidisciplinary | Rapid Review | Open Access Journal

Received August 3, 2017, accepted August 22, 2017, date of publication September 4, 2017, date of current version September 27, 2017.

Digital Object Identifier 10.1109/ACCESS.2017.2748621

Investigation of Energy Savings on Industrial Motor Drives Using Bidirectional Converters

IOANNIS KARATZAFERIS[1], (Student Member, IEEE), EMMANUEL C. TATAKIS[1], AND NICK PAPANIKOLAOU[2], (Senior Member, IEEE)

[1]Department of Electrical and Computer Engineering, University of Patras, 26504 Patras, Greece
[2]Department of Electrical and Computer Engineering, Democritus University of Thrace, 67132 Xanthi, Greece

Corresponding author: Ioannis Karatzaferis (jkaratzaferis@ece.upatras.gr)

ABSTRACT Motor drives is a widely used technology, offering many advantages, such as exceptional speed control and flexibility. Improvement of reliability and efficiency has become a great research interest. Toward this direction and considering the major recent developments in supercapacitor technology, the use of bidirectional energy recovery converters has been introduced in various industrial applications. In this paper, the regenerative braking of a three-phase induction motor controlled by a variable frequency drive will be analyzed and the portion of kinetic energy that can be recovered will be calculated. The main contribution of this paper is a methodology for the estimation of the energy savings that can be achieved from the use of such an energy recovery feature. In addition, the optimum braking duration that maximizes the recovered energy will be investigated. The analysis presented in this paper has been validated experimentally and the results are discussed.

INDEX TERMS Bidirectional power flow, DC-DC power converters, motor drives, energy efficiency, regenerative braking, regenerative energy storage device, supercapacitors.

I. INTRODUCTION

The use of variable frequency drives has increased greatly over the last years. The reasons behind this are, among others, controllability, good dynamic performance and flexibility [1]. Since the use of variable frequency drives has become such a popular solution for industry, their improvement in terms of efficiency and reliability is of great research interest.

There are a lot of electric drive controlled applications, such as lifts, tooling machines, packaging machines, etc. that are characterized by frequent stops/starts and intermittent duty cycles [2]; hence, there is a considerable energy saving potential by means of regeneration of the excessive kinetic energy during braking intervals. However, regenerative braking is not supported by typical variable frequency drives because they are usually supplied by diode bridge rectifiers. Thus, in this case the regenerated kinetic energy is dissipated by the aid of braking resistors. This can result in a significant energy loss amount, especially when stops/starts are frequent.

Another important issue is the ride-through capability [3]–[5]; in critical processes, the drive should withstand voltage sags that may last from a line cycle up to several minutes. This can be critical in specific industrial processes, where a single interruption may have serious impact on the production.

Several solutions have been proposed that employ bidirectional converters and appropriate energy storage technologies connected to the DC-bus of the drive, so that the excessive energy can be recovered and used again when necessary [3]–[12]. In this context, supercapacitor banks are usually preferred, due to the major developments of this technology over the recent years, whereas the converter topology that seems to be in favor for this application is the buck-boost bidirectional converter. In addition, several improvements on this topology have been proposed in order to achieve better performance and efficiency, such as the three-level buck-boost converter, or the interleaved soft-switching converters operating in discontinuous conduction mode (DCM) [7], [8]. However, there is only a limited number of studies concerning the energy saving that can be achieved by employing the proposed solutions; in [13] and [14], an analytical investigation on the optimal torque that should be applied during a speed transient, for improved energy recovery, is presented. However, the loss model for both the electrical and the mechanical losses is quite simple and moreover only a limited number of load cases is considered.

In the present work, a detailed study on the energy saving potential by employing a bidirectional energy recovery system is presented; the calculations are based on analytical

loss models during braking intervals and they are supported by experimental results. Moreover, the present analysis considers a wide range of loads in terms of nominal power and application type. In section II, a brief introduction to the energy recovery bidirectional converter and its control method is presented. In section III, the energy loss expressions of the drive system individual components are derived and a time-efficient method for the accurate calculation of the system total energy losses during regenerative braking intervals, by means of simulation, is proposed. In section IV the existence of an optimum deceleration duration that maximizes the recovered energy for any given electro-mechanical system is highlighted, supported by typical case studies and insightful discussion. Section V demonstrates an investigation on the energy savings that can be achieved using the proposed energy recovery system. The energy savings are strongly dependent on factors such as the electro-mechanical system moment of inertia, the speed profile of the application, etc. Finally, in section VI the proposed system and the braking duration optimization experimental verification is depicted. The laboratory setup as well as the results that support this paper are presented and useful conclusions are extracted.

II. BIDIRECTIONAL CONVERTER FOR ENERGY RECOVERY

In Fig. 1, a simple step-up/down topology commonly used for energy recovery and recuperation is shown. The high voltage side is connected to the drive DC-bus whereas the low voltage side is connected to the supercapacitor bank, since this energy storage technology is characterized by extremely high capacitance and low rated voltage. Different converter variations and control methods have been proposed in various publications [3]–[11]. The converter may operate either in continuous conduction (CCM), or in discontinuous conduction (DCM) mode. Operation in CCM means less current fluctuation within a switching cycle, thus less magnetic and switch turn-off losses. However, the control is generally more complex when the converter operates in CCM, requiring an extra (inner) current control loop. On the other hand, operation in DCM requires smaller inductance and offers fast dynamics and cycle by cycle current regulation, because in this mode the converter behaves as a current source. However, due to the increased current fluctuation in this mode, higher magnetic as well as conduction and turn-off losses occur [7], [11].

The most common method of controlling the converter operation is with the aid of simple voltage loops. The DC-bus voltage during normal motor operation does not exceed a value $V_{Bus,max}$, that corresponds to the rectified mains plus a tolerance for normal voltage fluctuations which is usually 10%. However, when a regenerative braking occurs, the motor is led to generator operation and its electrical power flows back to the drive, charging the DC-bus capacitance. The charging current has to be compensated by the bidirectional converter; thus, the bidirectional converter current reference is set by a voltage loop in order to regulate the DC-bus voltage at a reference value, $V_{Bus,ref}$. This value must

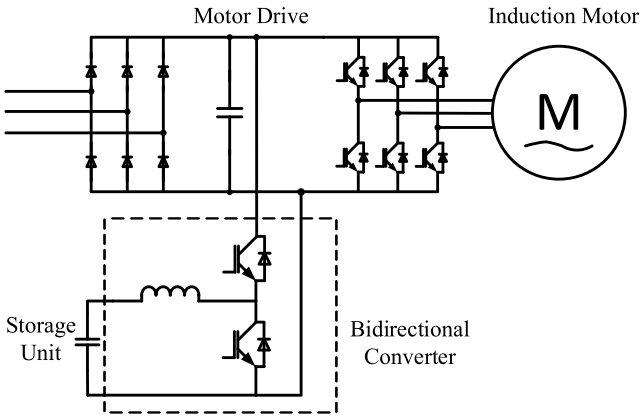

FIGURE 1. Drive system with bidirectional converter for kinetic energy recovery.

be above $V_{Bus,max}$ to avoid unnecessary converter operation during normal grid fluctuations. This simple control scheme is depicted in Fig. 2; the DC-bus voltage is compared to the reference value and the error is fed through a transfer function to define the current reference. If the DC-bus voltage is above the reference value the converter current reference is negative (current flows from the DC-bus to the storage unit). In the opposite case, the converter current reference is positive (current flows from the storage unit to the DC-bus).

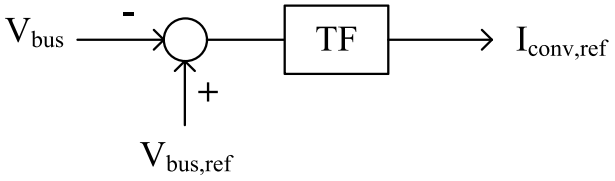

FIGURE 2. Bidirectional converter voltage control loop.

III. LOSSES DURING REGENERATIVE BRAKING

The total kinetic energy reduction (ΔE) during a deceleration is expressed by:

$$\Delta E = \frac{1}{2} J \left(\omega_{r,init}^2 - \omega_{r,final}^2 \right), \tag{1}$$

where J is the total moment of inertia of the drive system and $\omega_{r,init}$, $\omega_{r,final}$ are the initial and final rotor speeds. This kinetic energy cannot be fully recovered because of a number of energy losses, such as mechanical losses, $E_{loss,mech}$, electrical losses at the motor, $E_{loss,mot}$, inverter losses $E_{loss,inv}$, and finally, losses at the bidirectional energy recovery converter, $E_{loss,conv}$. The final recoverable kinetic energy amount, E_{rec}, can be estimated if all of the above mentioned losses are calculated and subtracted from the kinetic energy expressed in (1):

$$E_{rec} = \Delta E - E_{loss,mech} - E_{loss,mot} - E_{loss,inv} - E_{loss,conv} \tag{2}$$

A. MECHANICAL LOSSES

In this study, the term mechanical losses does not refer to the motor friction losses only, but it also includes the portion of the kinetic energy consumed by the mechanical load during the deceleration.

We will assume that the sum of the load torque, M_{Load}, and friction torque, M_{fr}, is expressed by (3), which covers most of the typical loads.

$$M_{Load}(\omega_r) + M_{fr}(\omega_r) = k_0 + k_1\omega_r + k_2\omega_r^2 \tag{3}$$

where k_0, k_1, k_2 are the load characteristic coefficients. The instantaneous mechanical power is expressed as:

$$P_{mech} = k_0\omega_r + k_1\omega_r^2 + k_2\omega_r^3 \tag{4}$$

Consequently, the mechanical losses during the deceleration are:

$$E_{loss,mech} = \int_{t_i}^{t_i+t_{br}} P_{mech}d\tau \tag{5}$$

where t_i and t_{br} are the starting time point and the duration of the regenerative braking respectively.

B. ELECTRICAL LOSSES

Electrical losses can be divided into motor, inverter, and bidirectional converter losses. To investigate these losses, the respective currents should be estimated. However, during the time interval t_{br} the motor currents are varying both in frequency and amplitude, therefore the losses cannot be calculated using standard formulas from the literature that assume steady state operation [15]–[17]. In order to calculate energy losses accurately, the motor currents during the deceleration interval are estimated by means of time simulation where the induction motor d-q model is employed (including the equivalent iron loss resistance), as shown in Fig. 3 [18]–[20]. The motor control is assumed to be scalar, therefore the deceleration is simulated by linearly decreasing the amplitude and frequency of the stator voltages, v_{qs} and v_{ds} while keeping a constant ratio between them. Having the values of the currents i_{qs} and i_{ds} estimated, the copper and iron instantaneous losses P_{Cu}, P_{Fe} can be calculated by:

$$P_{Cu} = \frac{3}{2}\left[\left(i_{qs}^2 + i_{ds}^2\right)R_s + \left(i_{qr}^2 + i_{dr}^2\right)R_r\right] \tag{6}$$

$$P_{Fe} = \frac{3}{2}\left(i_{di}^2 + i_{qi}^2\right)R_{Fe} \tag{7}$$

So, the total motor electrical losses during the deceleration can be calculated as:

$$E_{loss,mot} = \int_{t_i}^{t_i+t_{br}} (P_{Cu}(\tau) + P_{Fe}(\tau))d\tau \tag{8}$$

The braking interval t_{br} can be up to several seconds long, therefore the detailed simulation of the inverter and the bidirectional converter stages is time consuming. Thus, an alternative method to speed up the simulation is used. The braking interval, t_{br}, is discretized with a T_s (switching period) step; assuming that $t_{br} \gg T_s$, the ratio t_{br}/T_s can be rounded to the closest integer value without any significant error. In addition, if the switching frequency is sufficiently high the line currents are almost constant within a switching cycle. Under these assumptions the energy losses per switching cycle can be now calculated in a fast and effective manner. In more detail, the conduction losses over the k^{th} switching cycle, $k \in \left\{1, 2, \ldots, \frac{t_{br}}{T_s}\right\}$, are calculated by:

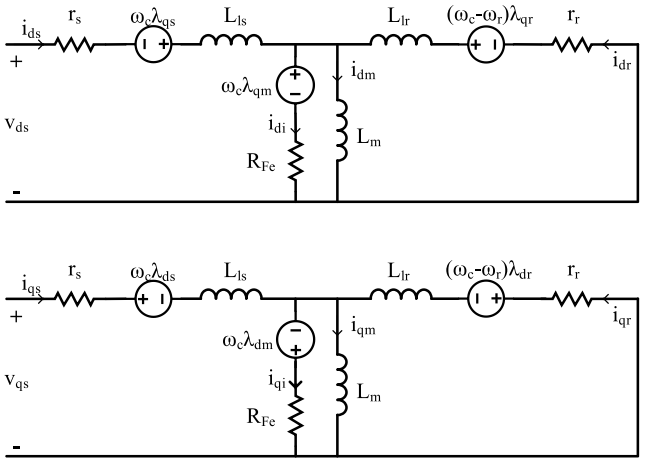

FIGURE 3. Induction motor D-Q model, including iron loss branch.

$$E_{cond,1ph}(k) = \left[v_{ce}\delta(k) + v_f(1-\delta(k))\right]i_{ph}(k)T_s \tag{9}$$

where v_{ce} and v_f are the forward voltages for the inverter IGBT switches and diodes respectively, δ is the inverter leg duty cycle which is expressing the relative conduction time of each switch and i_{ph} is the corresponding phase current, i_a, i_b or i_c, which is calculated by the dq/abc transformation of the stator i_{ds} and i_{qs} currents.

Finally, the switching losses for an inverter leg per switching cycle can be calculated by using the turn-on and turn-off energy, defined by the manufacturer of the device [21]–[23]. The turn-on $E_{on,1ph}$ and turn-off $E_{off,1ph}$ losses per inverter phase can be then expressed by (10), (11) respectively:

$$E_{on,1ph}(k) = E_{on\_Test}\frac{V_{Bus,ref}}{V_{Test}}\frac{i_{ph}(k)}{I_{Test}} \tag{10}$$

$$E_{off,1ph}(k) = E_{off\_Test}\frac{V_{Bus,ref}}{V_{Test}}\frac{i_{ph}(k)}{I_{Test}} \tag{11}$$

where E_{on_test}, E_{off_Test} are the turn-on and off losses derived by the devices technical data, whereas V_{Test}, I_{Test} are the test conditions for the determination of E_{on_test}, E_{off_Test} values. The DC-bus voltage is almost constant and equal to $V_{bus,ref}$ during the regenerative interval because it is regulated by the control loop in Fig. 2. The total inverter energy loss assuming a symmetrical load is expressed by (12):

$$E_{loss,inv} = 3\sum_{k=1}^{\frac{t_{br}}{T_{sw}}}\left(E_{cond,1ph}(k) + E_{on,1ph}(k) + E_{off,1ph}(k)\right) \tag{12}$$

The power flow from the inverter DC-bus to the bidirectional converter can be calculated by subtracting the inverter losses from the motor electrical power,

$$P_{conv,in} = P_{mot,el} - P_{inv,loss}, \tag{13}$$

where $P_{mot,el}$ is calculated by:

$$P_{mot,el} = \frac{3}{2}\left(v_{ds}i_{ds} + v_{qs}i_{qs}\right) \tag{14}$$

Moreover, the bidirectional converter average input current, I_{in}, is expressed by:

$$I_{conv,in} = \frac{P_{conv,in}}{V_{Bus.ref}} \tag{15}$$

An interleaved topology is more suitable for handling the high peak power during deceleration, therefore the use of an interleaved bidirectional converter is assumed. The input current is equally shared across the N bidirectional converter branches:

$$I_{in,branch} = \frac{I_{conv,in}}{N} \tag{16}$$

The bidirectional converter losses calculation is performed in a similar manner; the braking interval is discretized with a T_{sw} (bidirectional converter switching period) step; every discrete switching cycle is identified by the index $i \in \left\{1, 2, \ldots, \frac{t_{br}}{T_{sw}}\right\}$. For the power losses calculation the bidirectional converter duty cycle d and the intervals d_1 and d_2 (highlighted in Fig. 4) are required. In case of CCM operation, the duty cycle can be simply obtained from the input to output voltage ratio. However, this is not applicable in DCM operation because the converter operates as a current source; therefore, there is a direct relation between duty cycle and converter current. It is noted that even though losses calculations in this paper are performed for DCM operation, CCM operation can be analyzed in a similar manner. The equation set for losses calculation in DCM mode includes the following expressions:

$$I_{peak}(i) = \frac{d(i)T_{sw}\left(V_{Bus,ref} - V_o(i)\right)}{L} \tag{17}$$

$$I_{in,branch}(i) = \frac{d(i)I_{peak}(i)}{2} = \frac{d^2(i)T_{sw}\left(V_{bus,ref} - V_o(i)\right)}{2L} \tag{18}$$

$$d(i) = \sqrt{\frac{2LI_{in,branch}(i)}{T_{sw}\left(V_{bus,ref} - V_o(i)\right)}} \tag{19}$$

$$d_1(i) = \frac{I_{peak}(i)L}{T_{sw}V_o(i)} = \frac{d(i)\left(V_{Bus,ref} - V_o(i)\right)}{V_o(i)} \tag{20}$$

$$d_2(i) = (d(i) + d_1(i)) = \frac{d(i)V_{Bus,ref}}{V_o(i)}, \tag{21}$$

where V_o is the converter output (storage unit) voltage and L is the inductance of the converter. The IGBT switch current is equal to the branch input current, $I_{in,branch}$.

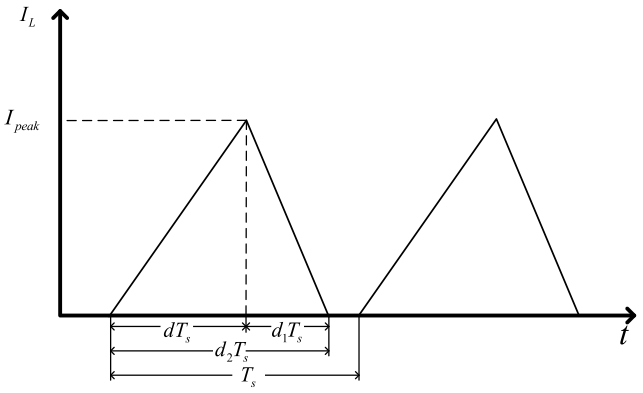

FIGURE 4. Inductor current for operation in DCM mode.

Moreover, (22), (23) stand for the diode and inductor average currents, respectively:

$$I_d(i) = \frac{I_{peak}(i)d_1(i)}{2} = \frac{I_{in,branch}(i)\left(V_{Bus,ref} - V_o(i)\right)}{V_o(i)} \tag{22}$$

$$I_L(i) = \frac{1}{2T_{sw}}I_{peak}(i)d_2 = \frac{d^2(i)T_{sw}(V_{Bus,ref} - V_o(i))V_{Bus,ref}}{2LV_o(i)} \tag{23}$$

Conduction losses, $E_{conv,cond}$, for the i^{th} converter switching cycle are then calculated by:

$$E_{conv,cond}(i) = \left(v_{ce,bb}I_{in,branch}(i) + v_{f,bb}I_d(i)\right)T_{sw}, \tag{24}$$

where $v_{ce,bb}$, $v_{f,bb}$ are the bidirectional converter IGBT and diode forward voltages, respectively. The turn-off losses are expressed by (25):

$$E_{off,conv}(i) = E_{off\_Test,conv}\frac{V_o(i)}{V_{Test,conv}}\frac{I_{peak}(i)}{I_{Test,conv}} \tag{25}$$

The inductor winding losses can be calculated using (26):

$$P_{wind}(i) = I^2_{L,rms}(i) \cdot R_L, \tag{26}$$

where R_L is the winding resistance and $I_{L,rms}$ is the inductor rms current, expressed by (27):

$$I_{L,rms}(i) = I_{peak}(i)\sqrt{\frac{d_2(i)}{3}} \tag{27}$$

The calculation of magnetic losses in DC-DC converters is a difficult task, because of the non-sinusoidal excitation. In various publications, different magnetic loss models for non-sinusoidal excited cores have been proposed [24]–[26]. In the current work, the generalized Steinmetz equation will be used for the estimation of the magnetic losses per switching cycle:

$$E_{core}(i) = V_e\frac{k_f\,(\Delta \mathrm{B}_i)^{\beta-\alpha}}{\mathrm{T}_{sw}}\sum_j\left|\frac{V_{ji}}{NA_e}\right|^a(\Delta t_{ji}), \tag{28}$$

where k_f, α, β are material coefficients, N is the number of turns, A_e, V_e are the core effective area and volume respectively, V_{ji} is the applied voltage during the j_{th} segment of the

i_{th} cycle and ΔB_i is the flux density fluctuation during the i^{th} switching cycle, which can be expressed by:

$$\Delta B_i = \frac{\left(V_{Bus,ref} - V_o(i)\right) d(i) T_{sw}}{N A_e} \tag{29}$$

Finally, the supercapacitor bank ESR losses per cycle are calculated by the following equation:

$$E_{ESR} = I_{o,rms}^2(i) R_{ES} T_{sw}, \tag{30}$$

where R_{ESR} is the equivalent series resistance of the supercapacitor bank and $I_{o,rms}$ is the converter output rms current. The output rms current calculation for a single branch converter is quite simple. However, in the case where an interleaved DC-DC converter is used for higher power handling capability, it can be quite complicated because as the individual branch currents add up, the output current ripple is reduced and its frequency is increased (Fig. 5).

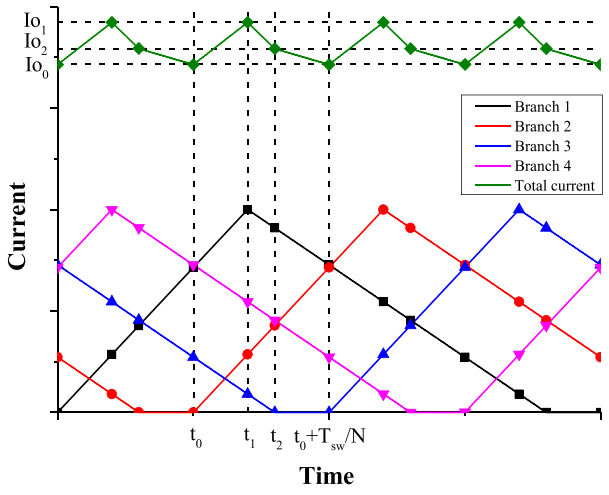

FIGURE 5. Individual branch currents and total output current of a 4-branch interleaved converter operating in DCM.

In [26]–[28] an analytical time domain method to determine the output current waveform is presented; initially, the time instances t_0, t_1, t_2 at which –as seen in Fig. 5 – the output current inclination changes, are determined. Afterwards, the output current value at these time points is calculated as the sum of the individual branch currents. The contribution of each branch is according to (31):

$$I_{branch,n}(t) = \begin{cases} \dfrac{(V_i - V_o)}{L}\tau & 0 < \tau < dTsw \\ \dfrac{I_{pk}}{d_1 T_{sw}}[d_1 T_{sw} - (\tau - dT_{sw})] & dT_{sw} < \tau < d_2 T_{sw} \\ 0 & \tau > d_2 T_{sw} \end{cases}$$
$$\tau = t + \frac{nT_{sw}}{N}, \tag{31}$$

where n is the branch index, $n \in \{1, 2, \ldots, N\}$. The output current rms value can be then calculated by the characteristic current values I_{o0}, I_{o1}, I_{o2} (also depicted in Fig. 5), using trivial mathematical formulas.

The total bidirectional converter losses per switching cycle can be found by summing all the above losses:

$$E_{conv}(i) = N\left(E_{conv,cond}(i) + E_{off}(i) + E_{wind}(i) + E_{core}(i)\right) + E_{ESR}(i) \tag{32}$$

Finally, the voltage of the supercapacitor bank has to be updated for the calculations of the next switching cycle:

$$V_o(i+1) = V_o(i) + \frac{P_{conv,in}(i) T_{sw} - E_{conv}(i)}{V_o(i) C} \tag{33}$$

The last term in (2) is then calculated by (34) and therefore the recoverable energy can be finally determined.

$$E_{conv,loss} = \sum_{i=1}^{\frac{t_{br}}{T_{sw}}} E_{conv}(i) \tag{34}$$

IV. OPTIMAL BRAKING DURATION

In every typical motor drive, the acceleration and braking durations are set by the user. The braking duration is associated with the motor torque and therefore with the motor, drive and bidirectional converter currents, affecting the energy losses during the deceleration. In this section, the optimal braking duration that minimizes the total losses will be investigated.

During braking, both the motor braking torque and the load torque force the load to decelerate according to (35):

$$M_e - M_{Load} - M_{fr} = J\frac{d\omega_r}{dt}, \tag{35}$$

where M_e is the motor electromagnetic torque (negative during a regenerative braking). The load torque acts as a damping factor, consuming the load kinetic energy during deceleration, whereas the motor torque is responsible for the regenerative braking process. Shorter deceleration duration means that more torque is applied by the motor for braking; thus, the stator, rotor, inverter and bidirectional converter currents are increased. This results in high electrical losses during the deceleration process. On the other hand, a longer deceleration interval would require less braking torque (thus lower currents), resulting in lower electrical losses. However, a larger portion of the load kinetic energy is now consumed by the load torque, increasing so mechanical losses.

This behavior is verified by means of the calculations presented in section III. The electrical and mechanical losses, as well as the recoverable energy amount were evaluated for different motor braking intervals. The effect of different loads and moment of inertia values can be examined by changing the load coefficients k_0, k_1, k_2 and the moment of inertia value, J. The case of a 4-pole, 55 kW induction motor-based system was considered. The motor parameters values that were considered for losses calculation are in Annex I. The system total moment of inertia is equal to $3.6 kgm^2$. The losses dependency on the braking duration can be studied in Figs 6, 7. Fig. 6 demonstrates a braking duration of 2.5 s whereas Fig. 7 demonstrates a duration of 0.75 s. The motor currents, as well as the calculated electrical and mechanical

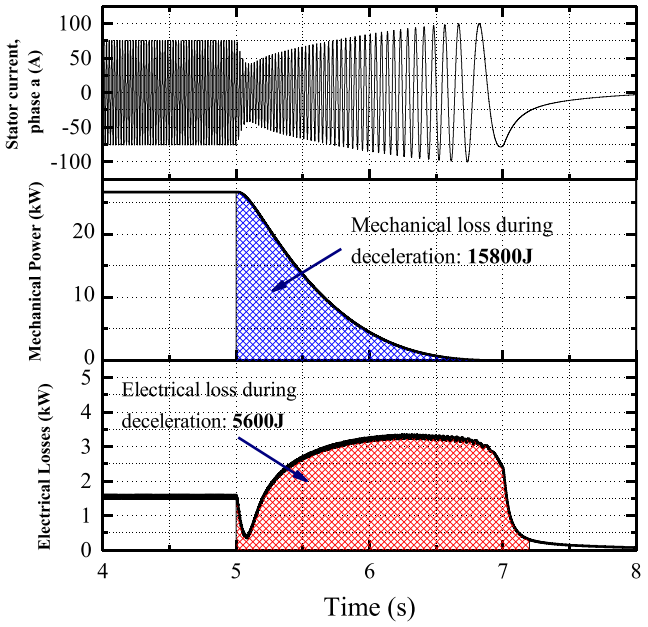

FIGURE 6. Stator current, Mechanical and Electrical losses for a 2.5 s deceleration interval. The initial kinetic energy is 40 *kJ*.

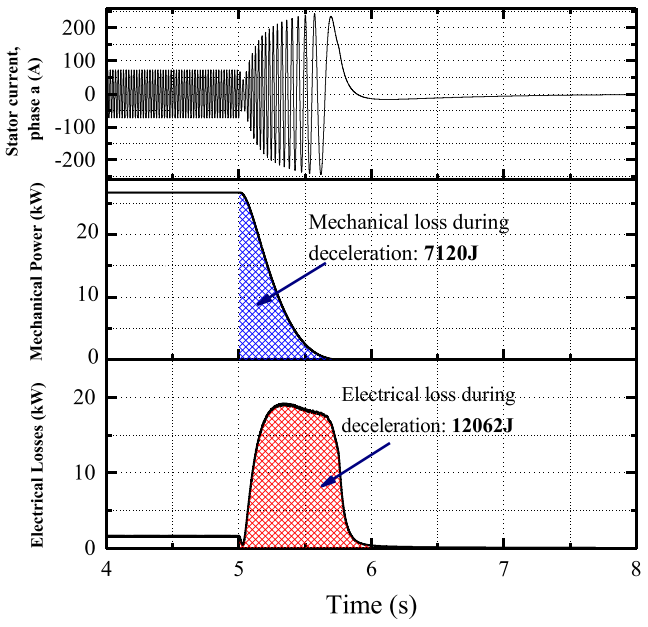

FIGURE 7. Stator current, Mechanical and Electrical losses for a 0.75 s deceleration interval. The initial kinetic energy is 40 *kJ*.

power losses are presented in both figures. The filled area under each curve represents the total energy loss during deceleration that is caused by the corresponding losses mechanism, either electrical or mechanical ones. In both cases the motor decelerates from full speed to zero, and the initial kinetic energy is 40 *kJ*. It can be clearly seen that in the first case, where braking is slower, a significant portion of the kinetic energy is consumed by the load, whereas in the second, more rapid one, the kinetic energy that is consumed by the load is reduced. However, the electrical losses are increased.

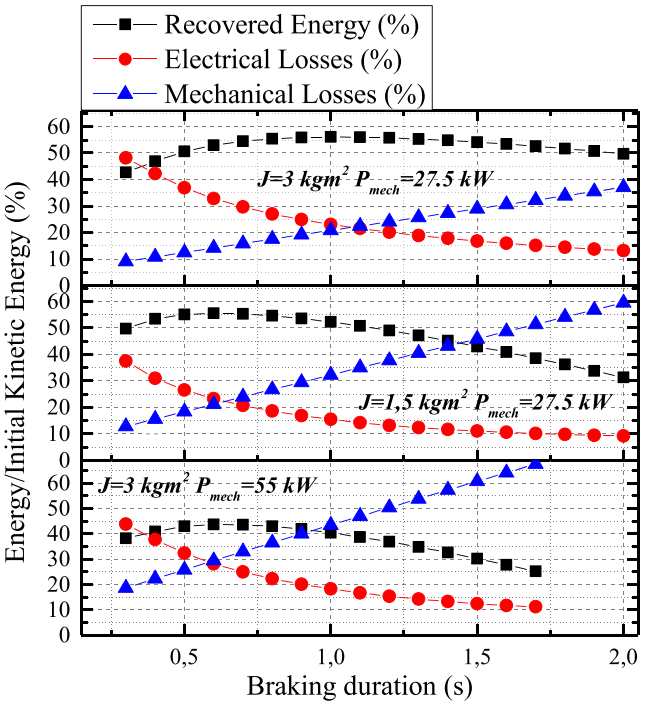

FIGURE 8. Search algorithm results for different load conditions and different load of inertia values.

Additionally, with the use of a search algorithm, multiple braking simulations are performed for a given system (applying various deceleration durations) and the optimal braking duration is determined. In Fig. 8 the results of the search algorithm are depicted. The recovered energy amount as well as the electrical and mechanical losses are expressed as a percentage of the load initial kinetic energy. The optimal braking duration dependency on factors such as the load power and total moment of inertia is also depicted. The results of the search algorithm for three different cases of output power and load moment of inertia are presented. According to those results, the load power clearly affects the optimal braking duration; heavier loads lead to high mechanical losses during deceleration and so the optimal braking duration decreases in order to minimize those losses. On the other hand, under light load conditions the optimal braking duration is longer, aiming to the reduction of the electrical losses. There is also a clear connection between the total moment of inertia value and the optimal braking duration; a higher moment of inertia value means that there is a greater amount of kinetic energy to be recovered and so a fast deceleration would provoke large motor currents and consequently significant electrical losses. Hence, the optimal braking duration becomes longer to comprise these losses and maximize the recovered energy.

V. ENERGY SAVING POTENTIAL

The mathematical formulation of the recoverable energy in section III is a flexible tool for the accurate estimation of the energy saving potential for any given drive system and any

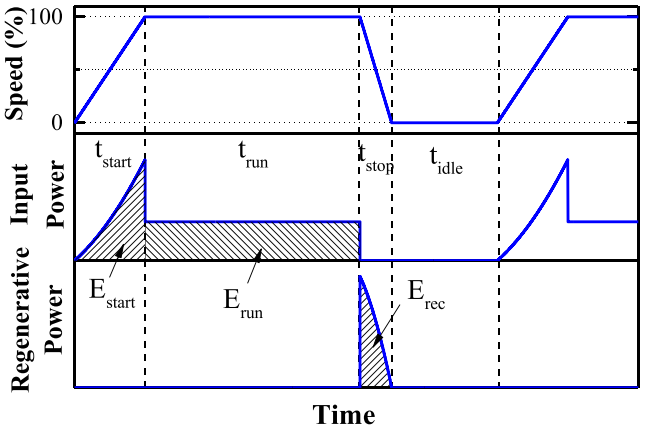

FIGURE 9. Investigation of energy saving potential.

periodic speed profile. Assuming a speed profile as depicted in Fig. 9, four time intervals can be distinguished depending on the drive state: motor starting interval, t_{start}, where E_{start} energy is consumed, normal running interval, t_{run}, where E_{run} energy is consumed, braking interval, t_{br}, where the energy recovery occurs, and idle interval, t_{idle}, where no energy is consumed. We can introduce the % energy saving index s, expressed as:

$$s = \frac{E_{rec}\eta_{ret}}{E_{start} + E_{run}} \tag{36}$$

where η_{ret} is the bidirectional converter efficiency during retrofit operation. Retrofit operation can occur when the motor is starting or running normally.

Energy saving depends greatly on parameters such as the load power and moment of inertia, the period of the speed profile and the profile duty cycle, which can be defined as the ratio of operating duration over the total period:

$$D = \frac{t_{start} + t_{run}}{t_{start} + t_{run} + t_{stop} + t_{idle}} \tag{37}$$

An investigation on the energy saving level as a function of those critical parameters can be performed for any given system; Figs 10a-10b show an investigation for the 55kW induction motor system of the previous example. According to these results, the period of the speed profile and the duty cycle value affect the run time and consequently the E_{run} amount, whereas the moment of inertia value affects greatly the recoverable energy E_{rec} and the starting energy E_{start}. Finally, as the mechanical power increases, E_{rec} decreases while E_{run}, E_{start} increase; therefore, the saving index s drops.

This analysis shows that there is a considerable potential for energy saving in industrial motor drive applications with the use of bidirectional energy recovery converters. Decisive factors for the energy saving level are –besides the braking duration – the load and speed profile characteristics.

VI. EXPERIMENTAL RESULTS

The bidirectional energy recovery converter as well as the theoretical energy saving calculations were verified by means

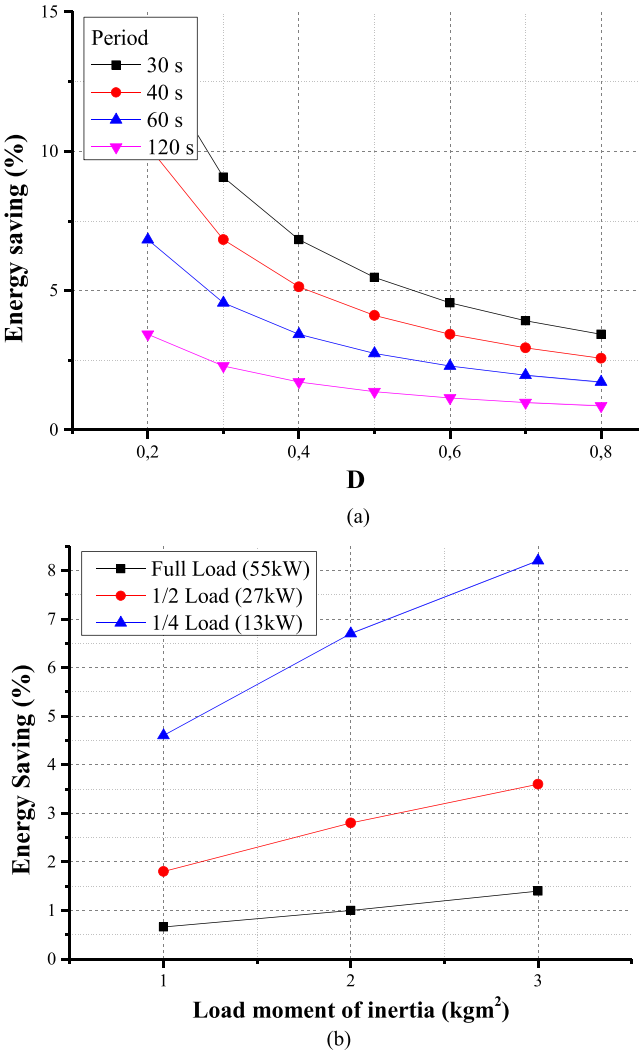

FIGURE 10. a. Investigation of the energy saving potential for 27 *kW* output power and 3 kgm^2 moment of inertia. b. Investigation of the energy saving potential for profile period 30 *s* and duty cycle *D=0.75.*

of a scaled experimental setup, consisting of a laboratory DC-DC converter prototype shown in Fig. 11 and a motor drive system with an emulated load, shown in Fig. 12. The drive supplies a 2-pole 4 kW induction motor and its technical specifications are noted in Annex I. The load was emulated by using a separately excited DC generator (which supplied a resistor bank), creating a linear speed-torque characteristic. The DC motor moment of inertia is equal to 0.006 $kg \cdot m^2$, resulting to a total 0.012 $kg \cdot m^2$ moment of inertia value for the electro-mechanical system. It is noted that the total moment of inertia value is not significantly high, however due to the high speed (3000 *rpm*) of the motor, the total kinetic energy is 860 *J* and therefore the motors can be used for a scaled experimental evaluation of the theory. On the other hand, the kinetic energy of this setup is not enough to justify the use of a supercapacitor bank and an interleaved converter; therefore, an electrolytic aluminum capacitor array and a single branch DC-DC converter operating in DCM were used.

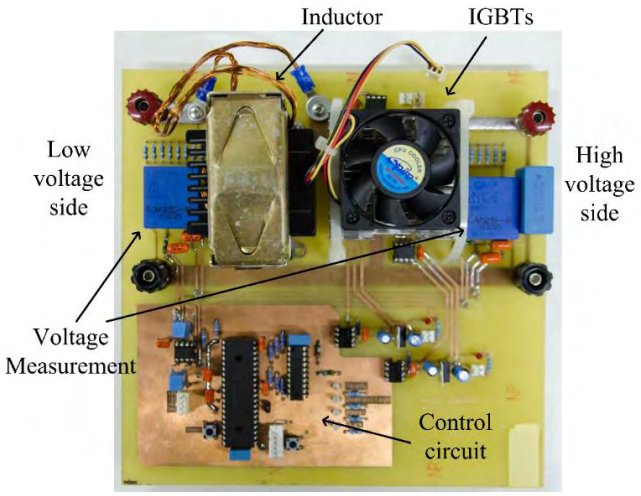

FIGURE 11. The experimental bidirectional DC-DC converter.

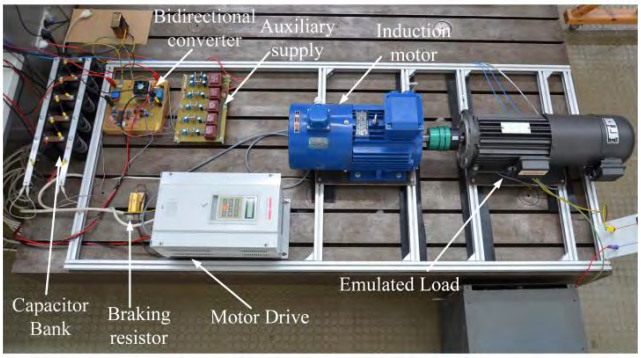

FIGURE 12. The experimental setup.

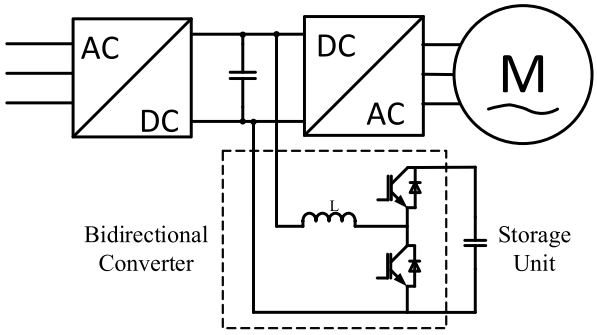

FIGURE 13. Alternative configuration for experiment.

The capacitor array consists of ten series/parallel connected 2.2 mF /450 V capacitors, resulting in a total capacitance of 5.5 mF /900 V.

Due to the use of electrolytic capacitors for this scaled experiment, an alternative configuration was considered, as presented in Fig. 13. In this configuration, the capacitor bank is connected at the high voltage side of the converter and its voltage is always higher than the DC-bus voltage. Therefore, step-up operation is required for energy recovery and step-down operation is required for energy recuperation.

FIGURE 14. Operation of the bidirectional DC-DC converter during a motor stop and operation for energy recuperation: capacitor bank voltage (upper waveform, 100V/div), DC-bus voltage (middle waveform, 100V/div) and inductor current (lower waveform, 5A/div).

An added benefit of this configuration is the lower current values at the energy storage unit side for a given power due to the high voltage, leading to reduced converter losses.

The experimental bidirectional converter consists of two 1200 V/30 A IGBTs and a 200 μH inductor, ensuring operation in DCM at 15 kHz switching frequency. The control of the converter is performed using a Microchip dsPIC30F4011 microcontroller. Typical voltage/current waveforms during the converter operation are presented in Fig. 14, where a regenerative braking as well as a retrofit operation interval are depicted. During regeneration, the DC-bus voltage rises because the recovered energy charges the DC-bus capacitor. As soon as this voltage exceeds the $V_{Bus,ref}$ value the bidirectional converter begins operation, storing the recovered energy in the capacitor bank (positive current means energy flow from the DC-bus to the capacitor bank). During regeneration, the capacitor bank voltage rise can be observed, indicating that energy is stored. Retrofit operation occurs when the motor restarts, indicated by the opposite current flow as well as the capacitor bank voltage drop.

For validation of the recoverable energy calculations in sections III-IV, various decelerations from full speed to zero were performed, applying different deceleration durations each time. The recovered energy was calculated by measuring the voltage of the capacitor bank before and after the regenerative braking. Moreover, the theoretically expected energy recovery was calculated by using the developed losses mathematical model. Fig. 15 demonstrates the comparison between the theoretical and the experimental results. A good concurrency between the experimental results and the theoretical calculations is noted, validating the effectiveness of the theoretical analysis. Moreover, the prediction of the optimum braking duration is fully verified, whereas for any duration between 0.2 s and 1 s the difference between experimental and theoretical values is lower than 5%.

Finally, for the validation of the energy saving potential investigation presented in section V, a periodic speed profile of 10 stops per minute was used as a speed reference for

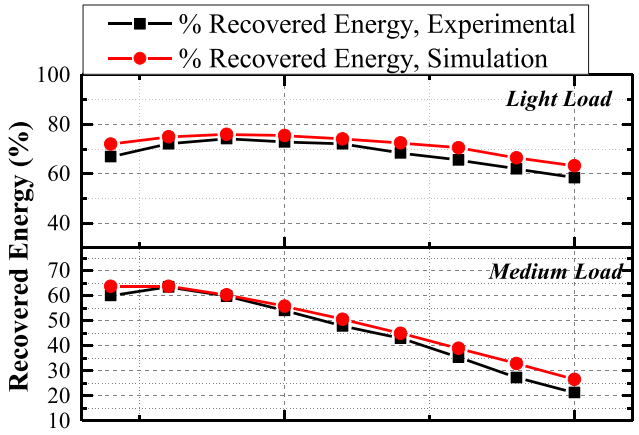

FIGURE 15. Recovered energy as a function of the deceleration duration. Theoretical versus experimental values for light and medium load.

TABLE 1. Comparison of energy consumption of a classic variable speed drive with and without using the proposed energy recovery converter.

	Energy consumption using braking resistor (Wh)	Energy consumption using energy recovery converter (Wh)	Measured improvement	Theoretical improvement
Operation under light load	12.54	11.41	9%	10%
Operation under medium load	36.52	35.5	2.7%	3.1%

the motor drive of the experimental setup, running continuously for two minutes. The drive consumption using the energy recovery converter was measured and compared to the conventional case of using a braking resistor. The consumption measurements were performed by the aid of a Zimmer LMG500 precision power analyzer and the results are summarized in Table 1; the measured energy saving level is similar to the calculated one, validating the theoretical approach in the current work.

VII. CONCLUSIONS

In this paper, a detailed study concerning the use of energy recovery bidirectional converters with typical industrial drives was presented. The energy losses during a regenerative braking interval were analyzed and an accurate estimation on the amount of the load kinetic energy that can be recovered as a function of the deceleration duration was presented. Finally, a method to estimate the energy saving that can be achieved using an energy recovery converter was presented. This can determine, in a reliable way, whether such an energy recovery feature is worth installing or not. A remarkable concurrency between the experimental results and the theoretical expectations was observed, validating the value of the presented theoretical analysis.

ANNEX I
SIMULATION AND EXPERIMENTAL PARAMETERS

See Table 2–5.

TABLE 2. Example motor parameters.

Nominal Power	55 kW
Number of Poles	2
Stator Resistance	0.04 Ω
Rotor resistance	0.15 Ω
Stator leakage inductance	0.5 mH
Stator leakage inductance	0.5 mH
Mutual inductance	0.0246 H
Iron loss resistance	94 Ω
Motor Moment of inertia	0.8 kg·m^2
Load Moment of inertia	2.8 kg·m^2

TABLE 3. Experimental setup motor parameters.

Nominal Power	4 kW
Number of Poles	2
Stator Resistance	1.95 Ω
Rotor resistance	1.191 Ω
Stator leakage inductance	5.4 mH
Stator leakage inductance	5.4 mH
Mutual inductance	0.3668 H
Iron loss resistance	920 Ω
Motor Moment of inertia	0.006 kg·m^2
Load Moment of inertia	0.006 kg·m^2

TABLE 4. Load coefficients used for simulation.

Nominal Load (55 *kW*)	k_2=0.015
½ Nominal Load (27.5 *kW*)	k_2=0.0075

TABLE 5. Load coefficients used for experiments.

Light load	k_0=0.45
Medium load	k_0=0.2, k_1=0.008

REFERENCES

[1] A. T. de Almeida, F. J. T. E. Ferreira, and D. Both, "Technical and economical considerations in the application of variable-speed drives with electric motor systems," *IEEE Trans. Ind. Appl.*, vol. 41, no. 1, pp. 188–199, Jan./Feb. 2005.
[2] M. A. Valenzuela, P. V. Verbakel, and J. A. Rooks, "Thermal evaluation for applying TEFC induction motors on short-time and intermittent duty cycles," *IEEE Trans. Ind. Appl.*, vol. 39, no. 1, pp. 45–52, Jan. 2003.
[3] A. von Jouanne, P. Enjeti, and B. Banerjee, "Assessment of ride-through alternatives for adjustable speed drives," in *Proc. IAS*, vol. 2. 1998, pp. 1538–1545.
[4] P. J. Grbović, P. Delarue, P. Le Moigne, and P. Bartholomeus, "The ultracapacitor-based controlled electric drives with braking and ride-through capability: Overview and analysis," *IEEE Trans. Ind. Electron.*, vol. 58, no. 3, pp. 925–936, Mar. 2011.
[5] T. Wei, S. Wang, and Z. Qi, "A supercapacitor based ride-through system for industrial drive applications," in *Proc. ICMA*, Aug. 2007, pp. 3833–3837.
[6] D. Vinnikov, I. Roasto, and J. Zakis, "New bi-directional DC/DC converter for supercapacitor interfacing in high-power applications," in *Proc. EPE/PEMC*, Sep. 2010, pp. T11-38–T11-43.
[7] Z. Junhong, L. Jih-Sheng, K. Rae-Young, and Y. Wensong, "High-power density design of a soft-switching high-power bidirectional DC-DC converter," *IEEE Trans. Power. Electron.*, vol. 22, no. 4, pp. 1145–1153, Jul. 2007.
[8] P. J. Grbović, P. Delarue, P. Le Moigne, and P. Bartholomeus, "A bidirectional three-level DC-DC converter for the ultracapacitor applications," *IEEE Trans. Ind. Electron.*, vol. 57, no. 10, pp. 3415–3430, Oct. 2010.
[9] P. J. Grbović, P. Delarue, P. Le Moigne, and P. Bartholomeus, "Modeling and control of the ultracapacitor-based regenerative controlled electric drives," *IEEE Trans. Ind. Electron.*, vol. 58, no. 8, pp. 3471–3484, Aug. 2011.

[10] C. Attaianese, V. Nardi, and G. Tomasso, "High performances supercapacitor recovery system for industrial drive applications," in *Proc. APEC*, vol. 3. Feb. 2004, pp. 1635–1641.
[11] I. Karatzaferis, E. Tatakis, and N. Papanikolaou, "Analysis and design of a universal energy recovery converter for use with industrial inverters," in *Proc. CPE*, Jun. 2015, pp. 234–239.
[12] N. Papanikolaou, J. Karatzaferis, M. Loupis, and E. Tatakis, "Theoretical and experimental investigation of brake energy recovery in industrial loads," *Energy Power Eng.*, vol. 5, no. 7, pp. 459–473, Sep. 2013.
[13] K. Inoue, K. Ogata, and T. Kato, "A study on an optimal torque for power regeneration of an induction motor," in *Proc. PESC*, 2007, pp. 2108–2112.
[14] K. Inoue, T. Kato, and K. Kotera, "Design methodology of optimal trajectories minimizing loss of induction motor under torque amplitude limit," in *Proc. COMPEL*, Jun. 2012, pp. 1–5.
[15] J. W. Kolar, F. C. Zach, and F. Casanellas, "Losses in PWM inverters using IGBTs," in *Proc. Elect. Power Appl.*, 1995, pp. 285–288.
[16] K. Zhou and D. Wang, "Relationship between space-vector modulation and three-phase carrier-based PWM: A comprehensive analysis [three-phase inverters]," *IEEE Trans. Ind. Electron.*, vol. 49, no. 1, pp. 186–196, Feb. 2002.
[17] B. Baodong and C. Dezhi, "Inverter IGBT loss analysis and calculation," in *Proc. ICIT*, 2013, pp. 563–569.
[18] J.-W. Choi, D.-W. Chung, and S.-K. Sul, "Implementation of field oriented induction machine considering iron losses," in *Proc. APEC*, vol. 1. Mar. 1996, pp. 375–379.
[19] G. O. García, J. A. Santisteban, and S. D. Brignone, "Iron losses influence on a field-oriented controller," in *Proc. IECON*, vol. 1. 1994, pp. 633–638.
[20] K. Matsuse, T. Yoshizumi, S. Katsuta, and S. Taniguchi, "High-response flux control of direct-field-oriented induction motor with high efficiency taking core loss into account," *IEEE Trans. Ind. Appl.*, vol. 35, no. 1, pp. 62–69, Jan. 1999.
[21] Z. Xuhui, W. Xuhui, G. Xinhua, and Z. Feng, "Analysis of voltage source inverter losses model," in *Proc. ICEICE*, 2011, pp. 5704–5707.
[22] A. Fratta and F. Scapino, "Modeling inverter losses for circuit simulation," in *Proc. PESC*, vol. 6. 2004, pp. 4479–4485.
[23] M. H. Bierhoff and F. W. Fuchs, "Semiconductor losses in voltage source and current source IGBT converters based on analytical derivation," in *Proc. PESC*, vol. 4. 2004, pp. 2836–2842.
[24] J. Reinert, A. Brockmeyer, and R. W. De Doncker, "Calculation of losses in ferro- and ferrimagnetic materials based on the modified Steinmetz equation," *IEEE Trans. Ind. Appl.*, vol. 37, no. 4, pp. 1055–1061, Jul./Aug. 2001.
[25] L. Jieli, T. Abdallah, and C. R. Sullivan, "Improved calculation of core loss with nonsinusoidal waveforms," in *Proc. IAS*, vol. 4. 2001, pp. 2203–2210.
[26] K. Venkatachalam, C. R. Sullivan, T. Abdallah, and H. Tacca, "Accurate prediction of ferrite core loss with nonsinusoidal waveforms using only Steinmetz parameters," in *Proc. COMPEL*, 2002, pp. 36–41.
[27] S. Zhang and X. Yu, "A unified analytical modeling of the interleaved pulse width modulation (PWM) DC-DC converter and its applications," *IEEE Trans. Power Electron.*, vol. 28, no. 11, pp. 5147–5158, Nov. 2013.
[28] P. Cervellini, P. Antoszczuk, R. G. Retegui, M. Funes, and D. Carrica, "Steady state characterization of current ripple in DCM interleaved power converters," in *Proc. CAMTA*, Aug. 2016, pp. 33–38.

IOANNIS KARATZAFERIS (S'08) received the Dipl.Eng. degree in electrical engineering from the University of Patras, Patras, Greece, in 2010, where he is currently pursuing the Ph.D. degree.

His thesis is on energy saving methods for motor drive systems. His research interests include motor drive systems, bidirectional converters, and switch-mode power supplies. He is a member of the Technical Chamber of Greece.

EMMANUEL C. TATAKIS received the Diploma degree in electrical engineering from the University of Patras, Patras, Greece, in 1981, and the Ph.D. degree in applied sciences from the University of Brussels, Brussels, Belgium, in 1989.

He is currently a Professor with the Department of Electrical and Computer Engineering, University of Patras. His teaching activities include power electronics and electrical machines. His research interests include switch-mode power supplies, electric drive systems and electric vehicles, renewable energy systems, power factor correction, resonant converters, voltage multipliers, and educational methods in electrical machines and power electronics.

Dr. Tatakis is a member of the European Power Electronics Association and the Technical Chamber of Greece.

NICK PAPANIKOLAOU (M'08–SM'10) received the Dipl.Eng. and Ph.D. degrees in electrical engineering from the University of Patras, Patras, Greece, in 1998 and 2002, respectively.

Prior to his academic career, he had been with Hellenic Electric Energy Industry for several years, where he was involved in major European transmission and generation projects. He is currently an Assistant Professor with the Department of Electrical and Computer Engineering, Democritus University of Thrace, Xanthi, Greece. His research interests include power electronics, renewable energy exploitation, distributed generation, energy saving, electric vehicles, and power quality improvement.

Dr. Papanikolaou is also a member of CIGRE and the Technical Chamber of Greece.